Impact of Small Particles onto Rubber Surfaces at Glancing Angles

J. C. ARNOLD

Department of Materials Engineering, University of Wales Swansea, Singleton Park, Swansea SA2 8PP, United Kingdom

Received 22 April 1996; accepted 1 November 1996

ABSTRACT: A study was made of the impact of small particles onto a rubber surface at glancing angles of incidence. The aim of the study was to investigate the validity of assumptions made in a model of erosive wear of rubber [J. C. Arnold and I. M. Hutchings, *J. Phys. D: Appl. Phys.,* **25,** A222 (1992)], though it also provided an interesting insight into the impact mechanics of small particles (between 320 and 110 μm) at high velocities (up to 160 m s^{-1}). The study centred around the direct measurement of the impulses (normal and tangential) imparted by a known quantity of erodent striking an unfilled natural-rubber surface. These impulses were measured using a strain-gauged system once the accelerating airstream had been diverted using the Coanda effect. This information, coupled with values of the impact length and width (from microscopic studies), enabled the following values to be determined: rebound resilience, coefficient of friction, average frictional force, time of contact, and predicted rebound angle. We found that viscoelastic effects were of considerable importance, with a certain degree of coupling between the normal and tangential components of the impact. Surprisingly little difference was seen when comparing spherical glass beads with angular silica particles. © 1997 John Wiley & Sons, Inc. J Appl Polym Sci **64:** 2199–2210, 1997

Key words: impact; rubber; viscoelasticity

INTRODUCTION

It has been known for a long time that soft elastomeric materials are among the materials most resistant to erosive wear by small particles.[1,2] A recent study[3] has established that the mechanisms of erosion of elastomers are dominated by the growth of fatigue cracks leading to material removal. With glancing angles, the mechanism is similar to that occurring during abrasion by a blade or a smooth indentor. A pattern of transverse ridges is formed which are subsequently deformed by impacting particles as they slide over the surface. This repeated deformation causes fatigue cracks to grow at the base of each ridge, and this is the rate-determining step in material removal. With normal impact, fatigue cracks propagate under the influence of surface frictional stresses during the particle impact. Where these cracks intersect, material removal occurs.

Semitheoretical models of both of these situations have recently been developed.[4,5] With both glancing impact and normal impact the models provided very good qualitative predictions, with the effects of most of the impact parameters (velocity, particle size, and impact angle) and the materials' properties (modulus, fatigue properties, and coefficient of friction) all being predicted successfully. Quantitative predictions, however, were not so good, with the erosion rates being predicted only to within an order of magnitude. One of the main difficulties with both of these models is in the theoretical treatment of the particle impact, especially at glancing angles. The impact of small particles onto a viscoelastic surface at high velocity and a glancing angle of impact is a situation that is far from simple to model. In

order to improve the models for erosion of elastomers, a more detailed picture of the nature of the particle impact was needed for critical examination of some of the assumptions implicit in the models. This paper describes a study aimed at characterizing the glancing impact of small particles onto elastomeric surfaces.

The model developed for erosive wear at glancing angles combines a theory developed for the abrasive wear of rubber by a blade[6] with a treatment of the particle impact. In order to apply the blade-abrasion model, it was necessary to derive from the impact model the values of the frictional force, contact width, and sliding distance. Initially, the Hertzian theory of the impact of a sphere onto an elastic halfspace was considered; however because the deformations involved in a particle impact during erosion are substantial, the assumptions implicit in using Hertzian theory are not valid. For this reason we decided to use the Boussinesq model of the indentation of a rigid flat-ended punch. Although this necessarily introduces differences in the stress distribution at the edge of the contact area, because the erosion model required the average contact stresses, this was not seen to be a significant problem. Other assumptions implicit in the model were that the particles are spherical, that the elastomer possesses a constant coefficient of friction, and that rolling motion and viscoelastic effects can be neglected.

One significant assumption in the model is that the normal and tangential components of the impact can be separated and treated completely independently. The model starts with an expression for the normal force of

$$F = \frac{2ERd}{(1 - \nu^2)}$$

where E is the tensile modulus, R is the particle radius, d is the displacement, and ν is the Poisson's ratio. This can be combined with the normal velocity component of an impacting particle to give the maximum deformation (d_f) as

$$d_f = \sqrt{\frac{mv^2(1 - \nu^2)}{2ER}}$$

and the time of contact (T_c) as

$$T_c = \sqrt{\frac{\pi^2 m(1 - \nu^2)}{2ER}}$$

where m is the particle mass and v the normal component of velocity. The tangential resistive force can be found from the normal force multiplied by a constant coefficient of friction, and this can be averaged over a particle impact to give the average tangential force. The distance slid can also be calculated by analyzing the tangential component of the equation of motion with the tangential resistive force, as above. These parameters will be discussed later.

In order to examine the validity of these assumptions, we felt it necessary to characterize the particle impact. One method of doing this would have been to measure the impact force and contact time directly (possibly by the use of a combination of piezzoelectric load cells and high-speed photography). However, such methods become more difficult and less accurate as the particle size decreases and the impact velocity increases, so this approach is limited to the use of relatively large particles. It is then possible to extrapolate the results obtained with large particles down to the case of small particles with the use of viscoelastic models of the polymer,[7] but this can be a complex process involving several assumptions (especially in the case of glancing angles). We therefore decided that attempts should be made to characterize the impact of the particles typically found under erosive conditions without the use of extrapolations. With such small particles (less than 300 μm in diameter) and high velocities (up to 160 m s^{-1}), direct measurements of contact times and impact forces are virtually impossible; some indirect method was needed.

The method we used to measure both the tangential and normal forces resulting from an impact was first to measure the mechanical impulse imparted by a known amount of erodent. From this, the impulse per particle was calculated. In order to convert this into the force per particle, information was needed about the time of contact. This was obtained from measurements of the sliding distance and the initial and final velocity of the particle (from the impulse measurements). The rebound angles were also measured by "capturing" the particles and analyzing the distribution of their locations. The exact details of the measurement techniques are given below. From the measured values, we calculated the frictional force, time of contact, and sliding distance, and compared them with the values predicted by the impact model. In this way it was possible to highlight the model's successes and weaknesses.

EXPERIMENTAL

Materials

The elastomer used in this study was an unfilled vulcanized natural rubber with a hardness of approximately 38 IRHD. This is the same material that was used in previously published works on erosion[3–5] [denoted NR(m)]. It has a relatively high resistance to erosive wear, along with a high rebound resilience when measured with large projectiles. The rubber was prepared in the form of 5-mm-thick sheets, from which samples 2 cm × 2 cm were cut using a well-lubricated scalpel. An unfilled styrene–butadiene rubber was also used in the original study, but the results with this material were similar to those with natural rubber so they are not discussed here in detail.

The impacting particles used were spherical glass beads sieved into narrow size ranges of 320 μm, 160 μm, and 110 μm diameter (Ballotini, English Glass Co. Ltd.). In order to make comparisons with erosion tests, more-angular silica particles of 120 μm diameter were also used.

Impulse Measurements

The impulse measurements were performed using the same gas-blast rig used for the erosion studies. This is described in detail elsewhere,[8] but basically consists of a compressed-air system that accelerates particles along a parallel-sided nozzle. The normal or tangential impulse imparted by a known quantity of erodent can be measured from the force acting on the sample. This force will equal the total impulse imparted by the particles striking the sample in 1 s. There is, however, one substantial problem in such measurement: the accelerating airstream will also contribute to the force on the sample. In order to measure the impulse from the particles alone, the effect of the airstream must be either eliminated or accounted for.

To accomplish this we used the Coanda effect, the phenomenon whereby a streamlined fluid will follow a curved surface. This has been used before in erosion studies at high temperature to remove the cooling effect of the airstream.[9] The end of the erosion nozzle was curved and the outer surface was removed. In this way the airstream followed the curved surface, leaving the particles free to travel directly to the sample.

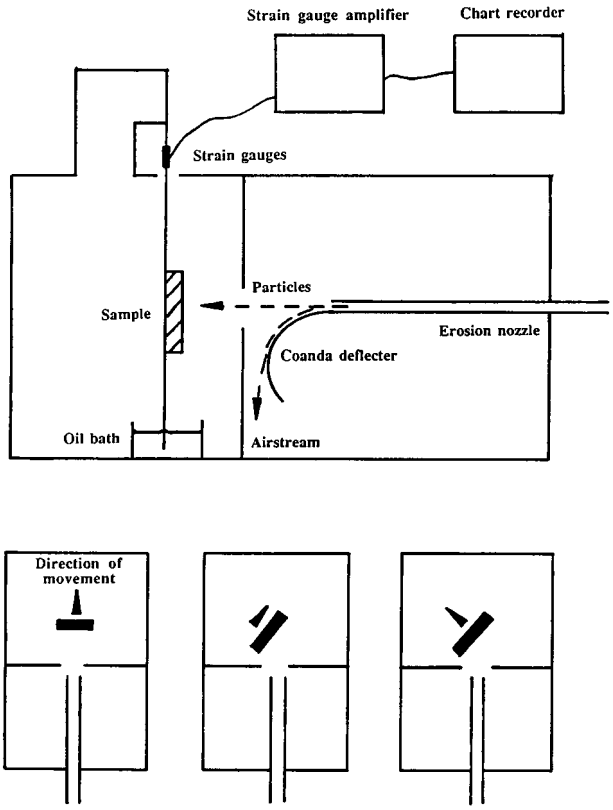

Figure 1 Side view of the experimental setup used to measure the impulses during erosion. Smaller diagrams are plan views of the three sample geometries used.

The experimental setup is shown in Figure 1. The Coanda nozzle was fabricated from a stainless-steel tube which was bent into the shape found to give the best deflection of the airstream, and the end of the tube was ground away to allow unhindered passage of the erodent particles. The nozzle and sample were positioned in a perspex chamber, separated by a plate with a central hole to prevent the deflected airstream from disturbing the sample. The sample was attached to a thin steel strip on which strain gauges were mounted. The strip was rigidly attached at the top and a damping system of a plate immersed in an oil bath was attached below the sample. The setup with the sample held vertically not only eliminated the need for calibration of the weight of the sample, but also prevented erodent particles from collecting on the sample. The deflection of the strip was measured by the strain gauges via an amplifier and chart recorder. Calibration of the system was performed by dead-loading the strip and measuring the deflection. We found that the load-deflection characteristics were virtually linear over the

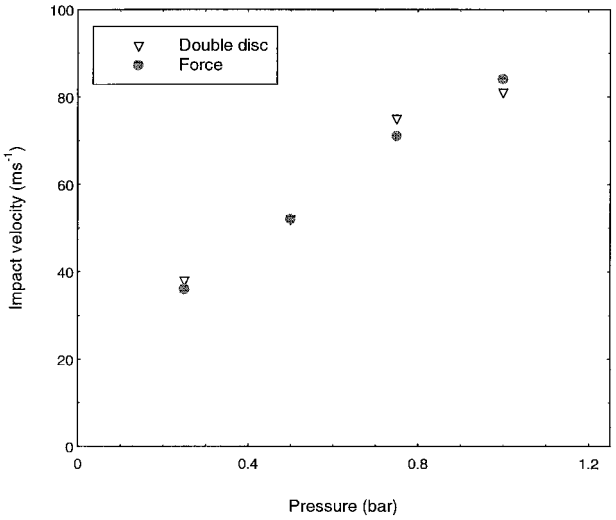

Figure 2 Variation of particle velocity with accelerating air pressure as measured by the double-disc method and the force method.

range used. Because the particle feed rate was not sufficiently controllable, the force was subject to fluctuations; so the total impulse imparted by a certain amount of erodent was measured from the area under the force–time curve.

The particle velocity was controlled by adjusting the accelerating air pressure and was measured by using a soft lead target. This has a restitution coefficient of virtually zero, so the impulse will equal the total initial momentum of the particles. The velocities measured in this manner were compared with those measured using the double-disk method[10] and were found to be in very close agreement (Fig. 2). This raises the possibility of the force method being used to measure particle velocities.

Three different sample orientations were used, illustrated in Figure 1. The first was to measure the normal impulse on a sample eroded at 90 degrees, the second to measure the tangential impulse on a sample eroded at 30 degrees, and the third to measure the normal impulse on a sample eroded at 30 degrees. Twenty grams of erodent were used for each test. We found that the overall reproducibility of the method was within ±5%.

Area of Contact

Because no observable damage is caused by single impacts, some other means was needed to determine the area of contact. Various methods of coating the sample and erodent particles were attempted, but we found that the best method was to observe the distribution of small fragments transferred from the erodent particles to the surface. Even with glass beads, there were enough of these fragments to mark the area of contact. The contact area was easily observable, either by optical microscopy or scanning electron microscopy (Fig. 3). The only remaining difficulty was to ensure that enough impacts occurred to measure the average contact area accurately but that there were not so many of them that individual impact sites were indistinguishable. The length and width of the contact area were measured over at least 10 individual impact sites and average values were taken from these measurements. The measured contact area included a small amount of nonsliding contact at the two ends of the contact area. This was accounted for analytically[11] and involved subtracting a small fraction of the contact area.

Rebound Angles

The method used to measure the rebound angles was one where, after impact, the particles struck a perspex plate coated with adhesive. The experimental setup is shown in Figure 4. The particles remained stuck to the perspex plate, allowing measurement of the angular distribution. Grid lines were scored on the perspex plate to enable the information to be converted into the number of particles per degree.

Coefficient of Friction

This is the first of several variables that can be determined indirectly from the measurements de-

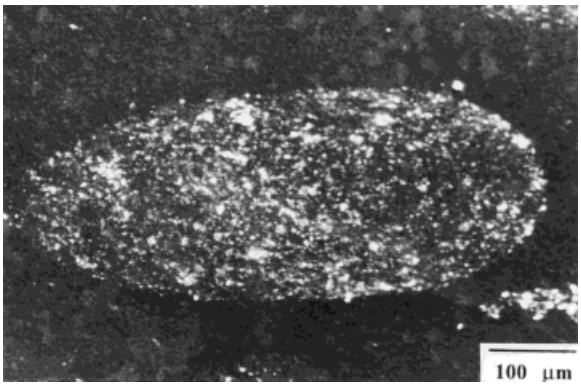

Figure 3 Scanning electron micrograph of an impact area produced by 160-μm glass beads at an impact angle of 30 degrees and a velocity of 70 m s^{-1}.

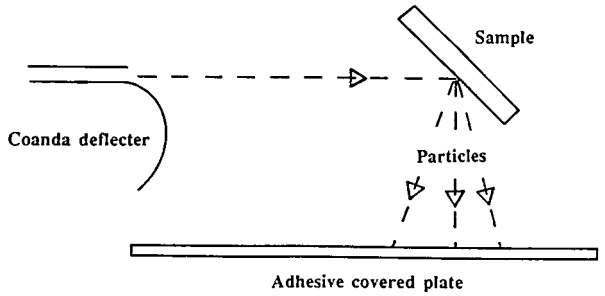

Figure 4 Experimental setup for measuring the particle rebound angle.

scribed above. The average coefficient of friction over an impact, μ, can be found simply from impulse measurements:

$$\mu = \left[\frac{\text{Impulse}_{(\parallel)}}{\text{Impulse}_{(\perp)}}\right]_{\text{at } 30^\circ}$$

where subscript ($\parallel$) indicates the impulse parallel to the surface, and subscript ($\perp$) is the impulse perpendicular to the surface.

Rebound Resilience

The rebound resilience at 90 degrees can also be determined. The initial particle velocity (v) is known, as is the rebound velocity (v') from the normal impulse. The rebound resilience can therefore be determined:

$$(\text{Rebound resilience})_{\text{at } 90^\circ} = \left(\frac{v'}{v}\right)^2_{\text{at } 90^\circ}$$

In order to determine the effect of adhesion, the normal impulse was measured on samples dusted with talcum powder.

It cannot be assumed that the same ratio of final and initial normal components of velocity exists for the case of glancing impact. Differences will almost certainly arise from the sliding motion of the particle. For this reason, a different value of the rebound resilience was determined at 30 degrees. The ratio of velocities was found from the initial normal component of velocity and the normal impulse at 30 degrees.

Average Force

From the tangential impulse at 30 degrees, the final particle velocity parallel to the surface [$v'_{(\parallel)}$] can be found. Coupling this with the initial tangential component of velocity [$v_{(\parallel)}$] and the distance slid (X_s) the average frictional force will be given by

$$F_{\text{av}} = \frac{m(v^2_{(\parallel)} - v'^2_{(\parallel)})}{2X_s}$$

where m is the mass of the impacting particle.

Time of Contact

The time of contact (T_c) can also be found from the initial and final velocities parallel to the surface and the distance slid:

$$T_c = \frac{2X_s}{(v_{(\parallel)} + v'_{(\parallel)})}$$

It is debatable whether this value, measured for the case of impact at 30 degrees, will be the same as that for normal impact. There are likely to be some differences, but in the absence of any more accurate measure the same value was used for both cases.

RESULTS AND DISCUSSION

Measurements of impulses and contact areas were made with glass beads (of 320, 160, and 110 μm diameter) and with 120-μm-diameter silica particles, all at velocities from 20 to 120 m s^{-1}. All three geometries of impulse measurement were used with the glass beads, whereas with silica particles the normal impulse at 90 degrees was not measured. Rebound angles were measured with the three sizes of glass beads at velocities between 30 and 40 m s^{-1}. These were compared with the values predicted using the final components of velocity derived from impulse measurements.

With Glass Beads

The results with glass beads are plotted in Figures 5 to 13 and show the following features:

1. The rebound resilience at 90 degrees was plotted against impact velocity for each of

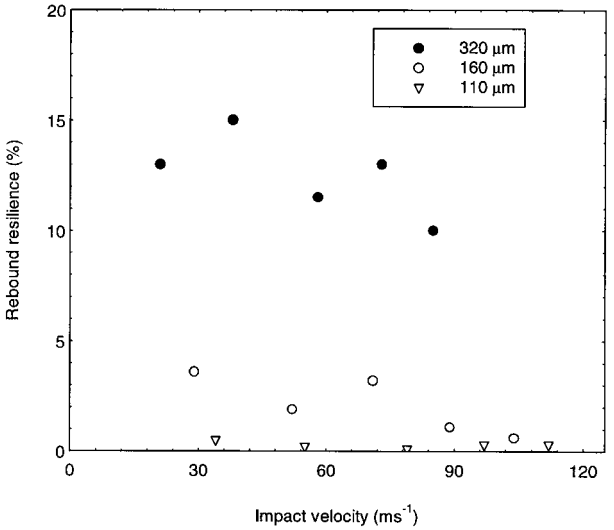

Figure 5 Variation of rebound resilience with impact velocity for normal impact of glass beads.

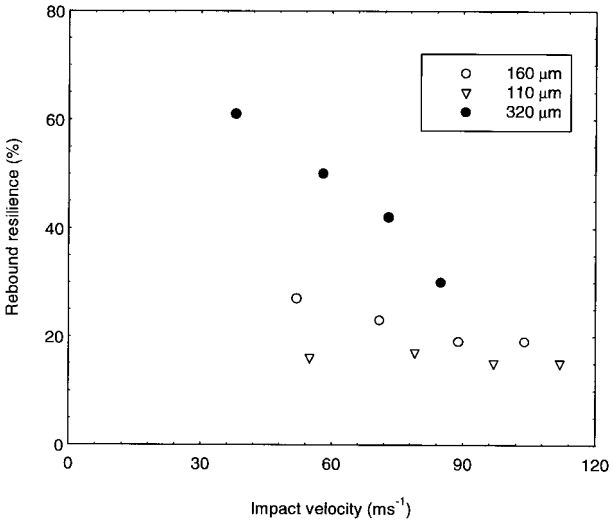

Figure 6 Variation of rebound resilience with impact velocity for the impact of glass beads at 30 degrees.

the sizes (Fig. 5). The resilience decreased with decreasing particle size, down to a very low value with the smallest particles. This initially surprising result was confirmed by the simple but inaccurate method of measuring the distance that the rebounding particles traveled horizontally before falling onto an adhesive-covered plate about 10 cm below the sample. It was thought that the low resilience might be due to adhesion; for small particles with a larger ratio of surface area to mass, the effect of adhesive forces would be larger. This was tested by dusting the sample with talcum powder before measuring the rebound resilience. The resilience was indeed higher with talcum powder, but not greatly (17% for 320-μm beads and 0.3% for 110-μm beads, as opposed to 11% and 0.1%, respectively, without talcum powder). The resilience also decreased slightly with increasing velocity (for the two larger sizes, at least) and it must be concluded that viscoelastic effects cause this and the variation with particle size.

2. The rebound resilience at 30 degrees, plotted against velocity (Fig. 6) also showed a decrease with decreasing particle size, though the effect was much less pronounced. The influence of velocity was also less clear; for large particles, a decrease in resilience was seen with increasing velocity, whereas with the small particles the effect was no greater than the experimental variation. The reasons for the higher values of resilience measured at 30 degrees compared with those at 90 degrees are not obvious. There seems to be some influence of the tangential deformations on the perpendicular impact dynamics, showing that resolving the impact into parallel and perpendicular components (as was done in the erosion model) may not be valid.
3. The distance slid is plotted against impact velocity in Figure 7. It can be seen that over the range of velocities used, the dis-

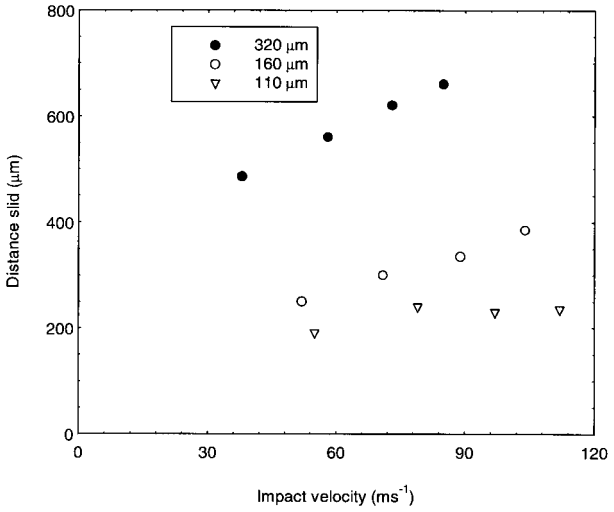

Figure 7 Distance slid plotted against the impact velocity for the impact of glass beads at 30 degrees.

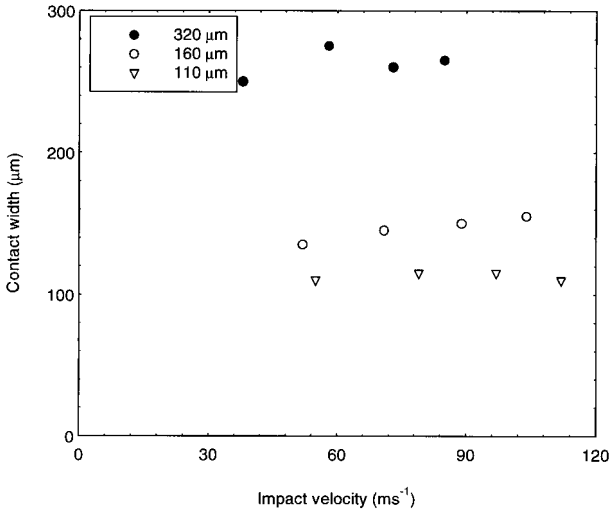

Figure 8 Contact width plotted against velocity for the impact of glass beads at 30 degrees.

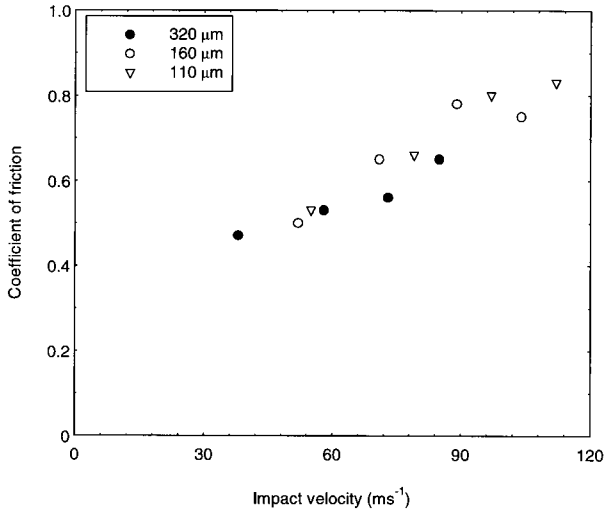

Figure 9 Coefficient of friction plotted against velocity for the impact of glass beads at 30 degrees.

tance the particle slid was between 1 and 3 times the particle diameter. The values increased with both velocity and particle size.

4. The width of the contact area is shown in Figure 8. This value is equal to the particle width for the 110-μm beads, but slightly smaller than the particle width and increasing with increasing velocity for the larger sizes. This shows that although the deformation was extensive, gross embedment did not occur. If embedment had occurred, the width of the contact area would equal the particle diameter over the whole range of velocities used.
5. The coefficient of friction, μ, is plotted against velocity for the three particle sizes in Figure 9. It is evident that μ is not constant, as was assumed in the erosion model, but in fact increases with sliding velocity. This effect is well known and can be attributed to higher viscoelastic energy losses at the higher velocities. The results for all three particle sizes superimposed onto a single curve. The only reason for a dependence on particle size would be a dependence on load, which, because contact occurs over the whole particle rather than just at asperities, is not likely to be important.
6. The average tangential force is shown in Figure 10. This force rose quite sharply with impact velocity and, not surprisingly, was larger with the larger particles.
7. The time of contact is plotted against impact velocity in Figure 11. As expected, these times were very short and decreased with particle size. There was also a marked decrease with increasing velocity. The theories of neither Boussinesq nor Hertz predict such a significant effect of velocity for normal impact, and it must be concluded that this result also was due to the interrelationship between the tangential and the normal deformations.
8. After calculating the time of contact, it is possible to replot the rebound resilience at 30 degrees (Fig. 12) against the time of

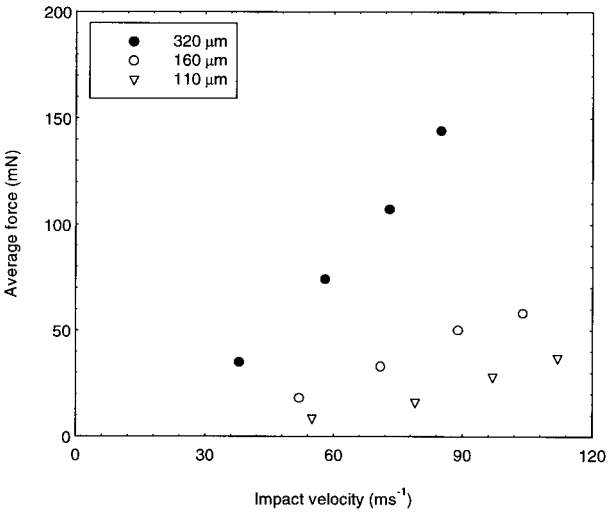

Figure 10 Average frictional force imparted by the impact of glass beads at 30 degrees.

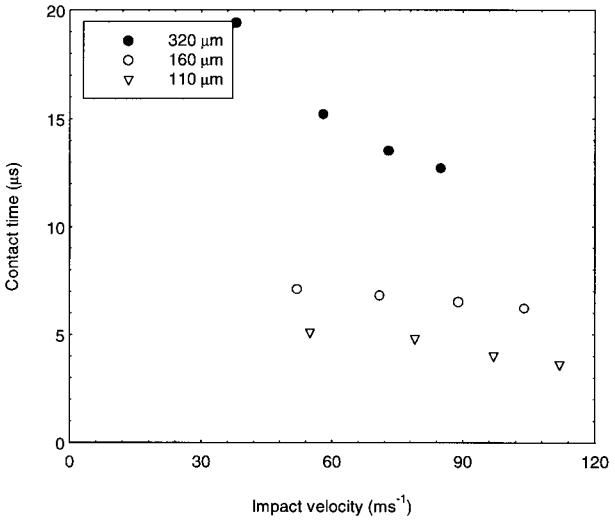

Figure 11 Time of contact plotted against velocity for the impact of glass beads at 30 degrees.

contact. This should then represent the viscoelastic behavior of the material. It can be seen that there was a decrease in resilience as the time of contact decreased (i.e., as the rate increased), mirroring the variation of the stored energy with rate which decreases to a minimum at the glass transition point. It would be interesting to observe whether the resilience rose with even smaller particles and hence times of contact.

9. Both the normal and parallel components of velocity at the end of the impact can be

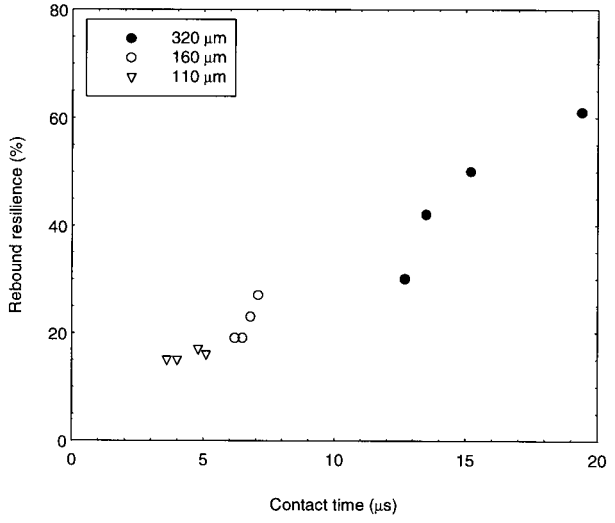

Figure 12 Rebound resilience at 30 degrees with glass beads plotted against the time of contact.

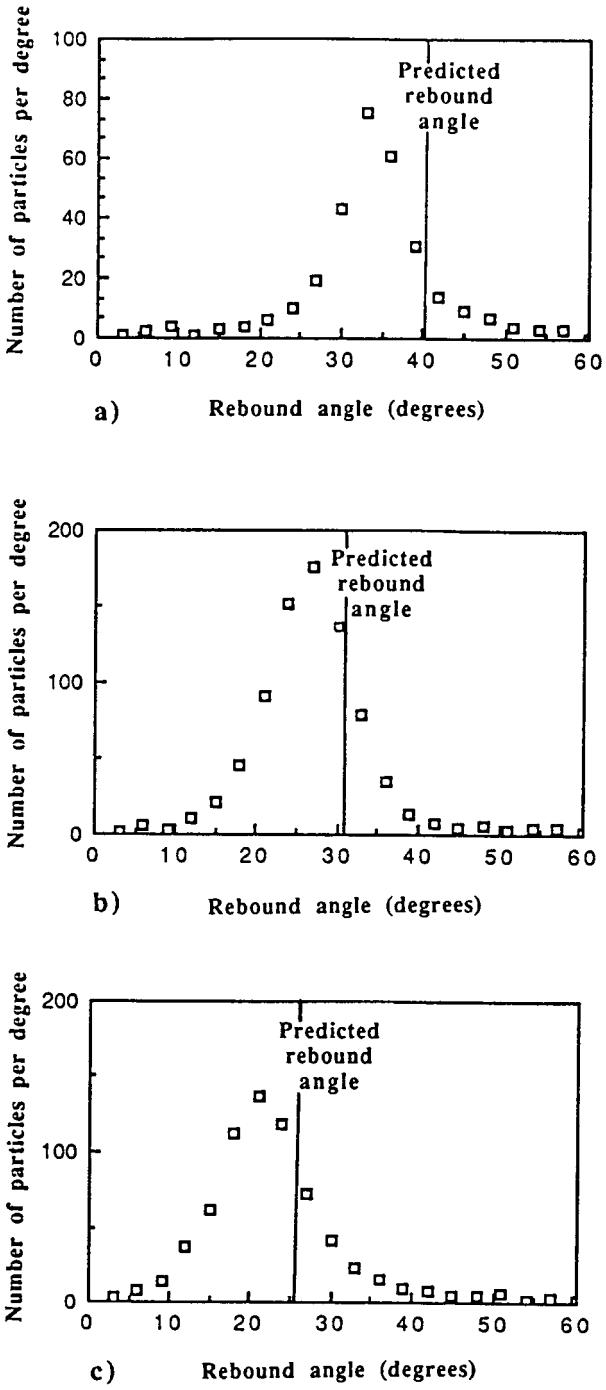

Figure 13 Comparison of the rebound angles predicted from the measured impulses and the actual rebound angles for the impact of glass beads at an impact angle of 30 degrees. (a) 320 μm; (b) 160 μm; (c) 110 μm.

determined from the measurements of impulses at 30 degrees, so the rebound angle can be predicted and compared with that measured experimentally (Fig. 13). The rebound angle (to the horizontal) was seen

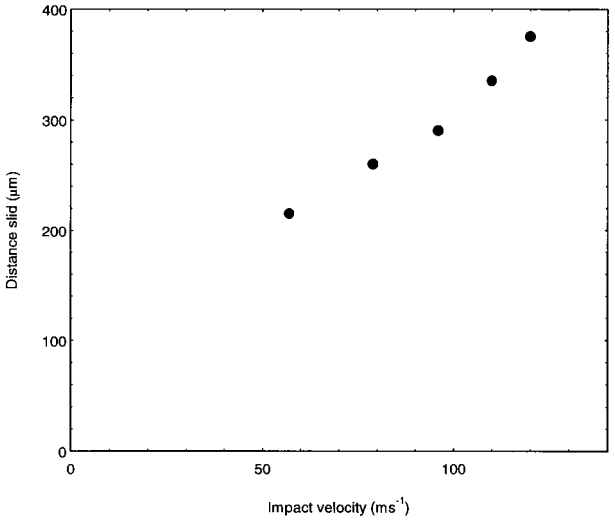

Figure 14 Distance slid plotted against the velocity for the impact of 120-μm silica particles at 30 degrees.

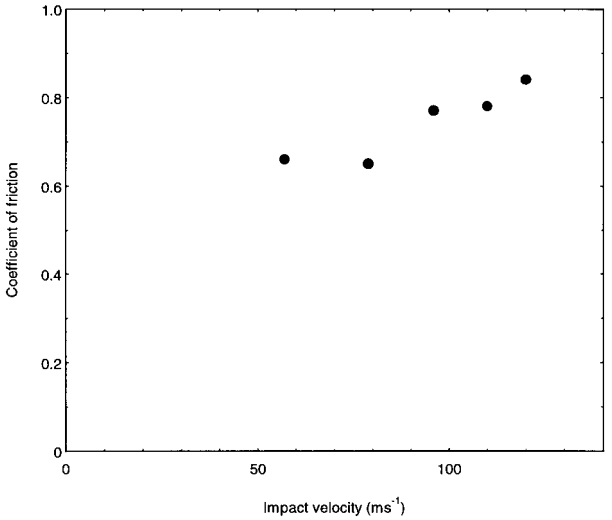

Figure 15 Coefficient of friction plotted against the velocity for the impact of 120-μm silica particles at 30 degrees.

to decrease with decreasing particle size, mirroring the predicted values. The slight discrepancy between the measured and predicted values is not particularly significant. It is also clear that the particles do exit in a forward direction without any excessive embedment.

With Silica

The results using 120-μm silica particles are shown in Figures 14 to 16. The following points are of importance:

1. The distance slid (Fig. 14) was slightly higher than with glass beads of a comparable size, with values ranging from 2 to 4 times the particle diameter.
2. The coefficient of friction (Fig. 15) was again seen to rise with increasing velocity and is comparable in size with that measured with glass beads.
3. The average force is plotted against velocity in Figure 16. As with glass beads, this force increased with velocity. It was thought that the effect of particle shape on erosion could be accounted for by a higher tangential force with the sharper silica particles. It is clear that this is not the case; the values of the average force are only slightly higher with silica particles than with glass beads of a similar size. The particle shape must therefore affect the process in some other way. Possible causes for this are discussed later.

Comparison of Theoretical and Measured Impact Characteristics

After measuring most of the important parameters involved in the particle impact, comparison can be made between the measured and predicted behavior. Such comparison should highlight the successes and failures of the erosion model.

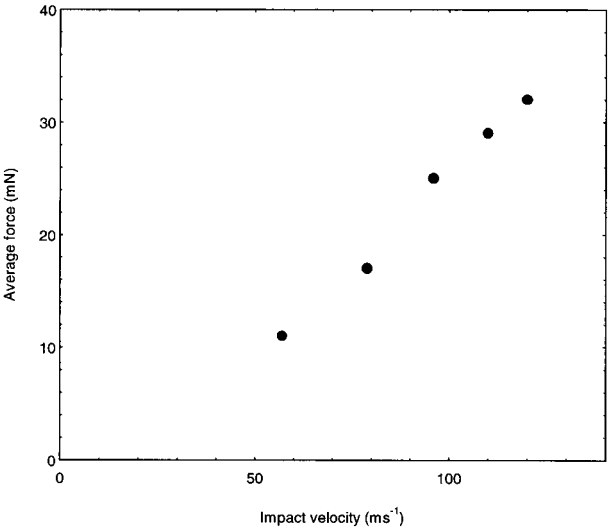

Figure 16 Average force per particle plotted against velocity for the impact of 120-μm silica at 30 degrees.

Coefficient of Friction

It was assumed initially that the coefficient of friction was constant. In fact, it has been found to vary considerably with sliding velocity, due to hysteresis losses. There is little dependence on particle size or shape. Such a variation could easily be accommodated into a revised erosion model.

Width of Contact Area

Assuming Boussinesq contact, the width of the contact area was taken as being equal to the particle diameter. It can be seen from Figure 8 that this approximation is reasonable: only at the lower end of the velocity range does the width decrease. It also emphasizes the point that Hertzian impact theory is not valid.

Time of Contact

The theory of Boussinesq predicts the time of contact as[4]

$$T_c = 7.9R\left[\frac{\rho(1-\nu^2)}{E}\right]^{1/2}$$

where R is the particle radius, ν the particle density, ν the Poisson's ratio of the rubber, and E the tensile modulus.

The ratio T_c/R should therefore be a constant, assuming the modulus does not vary. Plotting T_c/R against velocity (Fig. 17) shows plainly that this is not the case. Although the value of the ratio does not depend on the particle size, it was seen

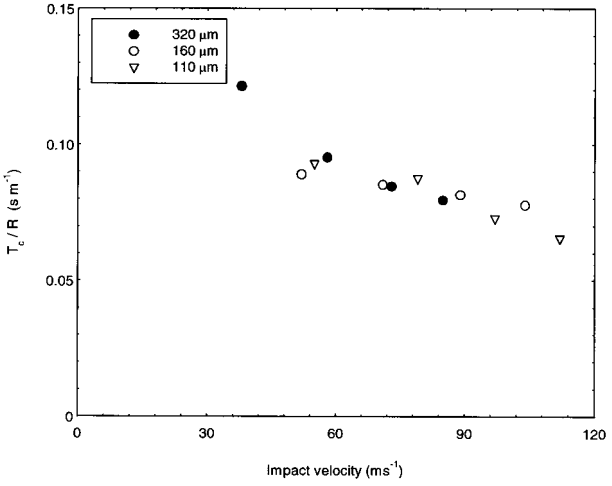

Figure 17 Value of T_c/R plotted against velocity for the impact of glass beads at 30 degrees.

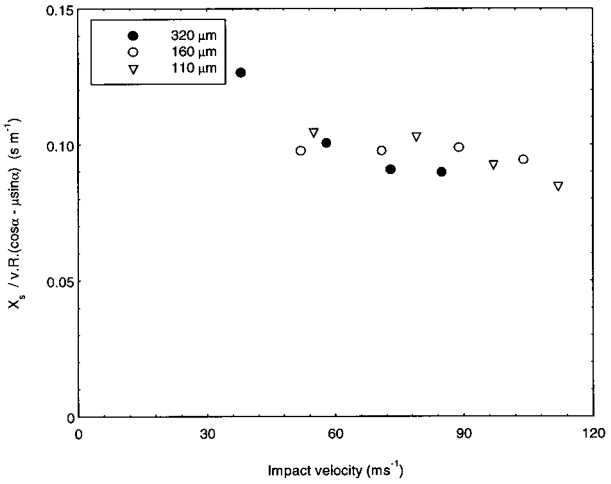

Figure 18 Value of $X_s/vR(\cos\alpha - \mu\sin\alpha)$ plotted against velocity for the impact of glass beads at 30 degrees.

to decrease with increasing sliding velocity. This effect, although due to the time-dependent nature of the mechanical properties (primarily the modulus, in this case), is not related to the impact time scale. Such a dependence would produce a variation with particle size. Rather, it seems to be concerned with the rate of deformation during sliding. This rate, dependent solely on the sliding velocity, appears to have some influence on the modulus in the vicinity of the impact area. This is not too difficult a concept to envisage; deformation at a high rate, from whatever cause, would be expected to lead to a higher modulus. The important point is that the interdependence of the normal impact deformation and the sliding deformation is once again illustrated.

Distance Traveled

From the erosion model, the distance traveled was taken as being[4]

$$X_s = 7.9vR(\cos\alpha - \mu\sin\alpha)\sqrt{\frac{\rho(1-\nu^2)}{E}}$$

where α is the impact angle (to the horizontal).

Assuming a constant coefficient of friction, the ratio X_s/vR would be expected to be a constant. However, it has been shown that μ varies with velocity. This can be accounted for by considering the ratio $X_s/vR(\cos\alpha - \mu\sin\alpha)$, which is plotted against velocity in Figure 18 (using the experimentally determined values of μ). It can be seen that this ratio decreases slightly with increasing

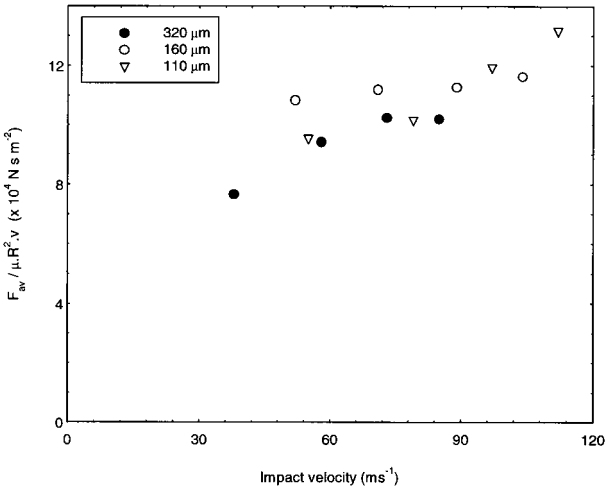

Figure 19 Value of $F_{av}/\mu R^2 v$ plotted against velocity for the impact of glass beads at 30 degrees.

velocity. This is presumably also due to the larger modulus seen at higher sliding velocities, as discussed above.

Average Tangential Force

The theoretical value for F_{av} is[4]

$$F_{av} = \mu R^2 v \sin \alpha \sqrt{\frac{E\rho}{1-\nu^2}}$$

The ratio $F_{av}/\mu R^2 v$, which should be a constant, taking the variable value of μ into account, is plotted in Figure 19. This ratio shows a general increase with increasing velocity and can again be attributed to a higher modulus at higher sliding velocities. The variation is in the opposite sense to that for T_c and X_s because F_{av} is proportional to $E^{1/2}$ as opposed to $E^{-1/2}$.

By comparing the values of the two ratios above, it is possible to determine values for ρ and $E/(1-\nu^2)$. This will therefore provide a valuable check on the validity of the impact model. Using the values at 80 m s^{-1} (and a value of ν equal to 0.5), this leads to ρ = 2.6 Mg m^{-3} (very close to the actual value of about 2.8 Mg m^{-3}) and E = 11.8 MPa (considerably higher than the low strain-rate value of about 1 MPa).

It is therefore apparent that if the variation of both μ and E with sliding velocity can be accounted for, the theory of Boussinesq impact holds remarkably well.

Rolling Motion

So far, we have assumed that the impacting particle travels with a pure sliding motion. Having measured the average tangential forces on the particle, it is possible to determine the extent of rolling motion that occurs. The results of such an analysis[11] show that by the end of the impact, pure rolling motion is occurring in all cases and that the distance that is slid (as opposed to rolled) is about one-third of the total distance traveled. This will obviously mean that approximating the tangential force as a constant (or as a sinusoidal variation) throughout the impact is not ideal; the force will be higher during the initial part of the impact, during the transition from sliding to rolling. The force will not reach zero when pure rolling occurs due to viscoelastic energy losses. The effect of this on the accuracy of the model is difficult to gauge without recourse to complex impact force measurements with larger particles. The fact that predictions from the impact model seem reasonable suggests that the effect is not great. It will, however, have a larger effect on the erosion behavior, because this is influenced much more strongly by the maximum tangential force. This is one of the main reasons for the quantitative discrepancies between the erosion model and experimental results.

Particle Shape

One of the other major assumptions in the erosion model is that the particles are spherical, even though it is known that the particle shape has a considerable influence on the erosion behavior.[11] The fact that the impact values obtained with spherical glass beads and with angular silica are very similar shows that this approximation is valid (presumably due to the fact that because contact occurs over the whole of the particle, the difference in shape is not significant). It does, however, leave the influence of particle shape on erosion behavior unexplained. It seems, from a study of the worn surface features,[11] that the particle shape has an effect on the wear process that is not accounted for in the model of blade abrasion. This is the other major cause of discrepancy between the erosion model and experimental results.

CONCLUSIONS

Measurements were made of the normal and tangential impulses imparted onto an unfilled natural-rubber surface by the impact of small glass beads and silica particles (between 320 and 110

μm in diameter) traveling at velocities up to 120 m s^{-1}. Combining these with measurements of the contact areas allowed a detailed characterization of the impact of small particles at glancing angles onto a rubber surface. The following important points were confirmed:

1. There is extensive deformation, with particles penetrating to depths greater than the particle radius. For this reason, a Hertzian analysis of the impact is not valid. The particles do not, however, become totally embedded and they exit in a forward direction.
2. Appreciable rolling motion occurs, with complete rolling occurring by the end of the impact in all cases.
3. The rebound resiliences are very low with the smallest particles used, showing that appreciable viscoelastic losses occur at these high rates of deformation.
4. The coefficient of friction is between 0.4 and 1 and increases with increasing sliding velocity due to viscoelastic losses. There is little influence of particle size or shape on the value of μ.
5. There is a considerable influence of the tangential deformation upon the normal deformation. A high sliding velocity causes the modulus of the rubber to be higher (due to viscoelastic effects). Apparently not just a localized effect, this influences the normal component of the impact, giving a shorter time of contact and distance travelled and a higher average force than would otherwise be expected. This interrelationship makes it clear that resolving a glancing impact into normal and tangential components is not necessarily a safe thing to do.
6. The modulus of the rubber under erosive conditions is roughly 10 times higher than that measured quasistatically due to the very high rates of loading.
7. Assuming the variation of modulus and coefficient of friction can be accounted for, an impact model based on Boussinesq geometry of a rigid flat-ended punch holds very well.

REFERENCES

1. V. K. Agarwal, D. Mills, and J. S. Mason, *Proc. 6th Int. Conf. on Erosion by Liquid and Solid Particle Impact,* J. E. Field and N. S. Corney, eds., Cavendish Laboratory, Cambridge, 1983.
2. S. Soderberg, S. Hogmark, V. Engman, and H. Swahn, *Tribology Int.,* **14,** 1979 (1981).
3. J. C. Arnold and I. M. Hutchings, *Wear,* **138,** 33 (1990).
4. J. C. Arnold and I. M. Hutchings, *J. Phys. D: Appl. Phys.,* **25,** A222 (1992).
5. J. C. Arnold and I. M. Hutchings, *Wear,* **161,** 213 (1993).
6. E. Southern and A. G. Thomas, *Plastics and Rubber: Materials and Applications,* **3,** 133 (1978).
7. E. Southern and A. G. Thomas, *J. Appl. Polym. Sci.,* **16,** 1641 (1972).
8. I. M. Hutchings, D. W. T. Deuchar, and A. H. Muhr, *J. Mater. Sci.,* **22,** 4071 (1978).
9. K. H. Yee, P. J. Shayler, and N. Collings, *Wear,* **91,** 161 (1983).
10. A. W. Ruff and L. K. Ives, *Wear,* **35,** 195 (1975).
11. J. C. Arnold, Ph.D. thesis, University of Cambridge, 1989.